Received: 9 January 2022 | Revised: 8 June 2022 | Accepted: 9 September 2022

DOI: 10.1002/gdj3.180

Geoscience Data Journal RMetS WILEY

DATA ARTICLE

One year of spectroscopic high-frequency measurements of atmospheric CO_2, CH_4, H_2O and $\delta^{13}C$-CO_2 at an Australian Savanna site

Niels C. Munksgaard[1] | **Ickjai Lee**[2] | **Thomas Napier**[2] | **Costijn Zwart**[1] | **Lucas A. Cernusak**[3] | **Michael I. Bird**[1]

[1]Earth and Environmental Science, College of Science and Engineering, James Cook University, Smithfield, Queensland, Australia

[2]Information Technology, College of Science and Engineering, James Cook University, Smithfield, Queensland, Australia

[3]Zoology and Ecology, College of Science and Engineering, James Cook University, Smithfield, Queensland, Australia

Correspondence
Niels C. Munksgaard, Earth and Environmental Science, College of Science and Engineering, James Cook University, Smithfield, QLD, Australia.
Email: niels.munksgaard@jcu.edu.au

Funding information
Australian Research Council, Grant/Award Number: LE110100144

Abstract

We provide a 1-year dataset of atmospheric surface CO_2, CH_4 and H_2O concentrations and $\delta^{13}C$-CO_2 values from an Australian savanna site. These semi-arid ecosystems act as carbon sinks in wet years but the persistence of the sink in dry years is uncertain. The dataset can be used to constrain uncertainties in modelling of greenhouse gas budgets, improve algorithms for satellite measurements and characterize the role of vegetation and soil in modulating atmospheric CO_2 concentrations. We found pronounced seasonal variations in daily mean CO_2 concentrations with an increase (by 5–7 ppmv) after the first rainfall of the wet season in early December with peak concentrations maintained until late January. The CO_2 increase reflected the initiation of rapid microbial respiration from soil and vegetation sources upon initial wetting. As the wet season progressed, daily CO_2 concentrations were variable, but generally decreased back to dry season levels as CO_2 assimilation by photosynthesis increased. Mean daily concentrations of CH_4 increased in the wet season by up to 0.2 ppmv relative to dry season levels as the soil profile became waterlogged after heavy rainfall events. During the dry season there was regular cycling between maximum CO_2/minimum $\delta^{13}C$-CO_2 at night and minimum CO_2/maximum $\delta^{13}C$-CO_2 during the day. In the wet season diel patterns were less regular in response to variable cloud cover and rainfall. CO_2 isotope data showed that in the wet season, surface CO_2 was predominantly a two-component mixture influenced by C_3 plant assimilation (day) and soil/plant respiration (night), while regional background air from higher altitudes represented an additional CO_2 source in the dry season. Higher wind speeds during the dry season increased vertical mixing compared to the wet season. In addition, night-time advection of high-altitude air during low temperature conditions also promoted mixing in the dry season.

Dataset

Available at figshare: https://figshare.com/s/9eef6231a818bb27b104. DOI: https://doi.org/10.6084/m9.figshare.17870939. 10 files with monthly data at 1 min intervals, 1 file with daily average data, 1 file with monthly maximum and minimum data, 1 file with meteorological data.

KEYWORDS
atmospheric CO_2, CH_4, NE Australia, savanna, $\delta^{13}C$-CO_2

1 | INTRODUCTION

Surface measurements of atmospheric CO_2 and CH_4 concentrations provide critical data necessary to validate and interpret remotely sensed greenhouse gasses (GHGs) and to characterize carbon sinks and sources within different ecosystems. An improved understanding of sinks and sources, in turn, helps establish more accurate carbon budgets at various temporal and spatial scales as part of national GHG accounting and reporting obligations.

In Australia, carbon budgets have been investigated using large scale ecosystem models as well as atmospheric transport inversion models (Haverd et al., 2013, 2015; Poulter et al., 2014; Villalobos et al., 2020, 2021). These studies have revealed significant interannual variations in the strength of terrestrial carbon sinks, and high uncertainties in the estimate of net primary productivity (NPP) in savanna lands. These semi-arid ecosystems are widespread across northern Australia and act as substantial carbon sinks in wet years but the persistence of these sinks in dry years is uncertain (Villalobos et al., 2021).

To help constrain uncertainties in modelling and accounting, there is a need for higher resolution GHG data, on the temporal and spatial scales of weather systems (Agustí-Panareda et al., 2019). Currently, there is a relative paucity of comprehensive, ground-based observations in the southern hemisphere including on the Australian continent. Less than 20% of sites monitored by the World Data Centre for Greenhouse gasses (WDCGG, https://gaw.kishou.go.jp/) and the Total Carbon Column Observing Network (TCCON, https://tccondata.org) are in the southern hemisphere. In Australia, there are 3 WDCGG sites for surface monitoring and 2 TCCON sites for atmospheric column monitoring. In addition, there are some 25 sites across Australia where local energy, CO_2 and water exchange between the atmosphere and a variety of ecosystems are observed via micrometeorological measurements (eddy covariance towers) as part of the OzFlux network (https://ozflux.org.au/).

Here we make available to the atmospheric modelling community a one-year record (June 2020 to May 2021) of laser spectroscopy measurements of atmospheric surface CO_2, CH_4 and H_2O concentrations and $\delta^{13}C$-CO_2 values from a savanna site in north-eastern tropical Australia. We present concentration and isotope data as 30-min running averages at 1-min intervals and as daily averages. We also provide 10-min wind data at three heights, as well as temperature and humidity measured at the same site.

The inclusion of high-frequency $\delta^{13}C$-CO_2 data enables the deconvolution of multiple carbon sources and sinks when modelling key carbon cycle processes (Graven et al., 2017) and helps characterize the role of vegetation and soil carbon in modulating atmospheric CO_2 on sub-daily and longer time scales. We are not aware of any previous publication of long-term, high-frequency spectroscopic $\delta^{13}C$-CO_2 data from an Australian site, but $\delta^{13}C$-CO_2 data based on flask sampling is available at weekly to monthly intervals from the three WDCGG Australian sites.

Finally, we comment on the seasonal and diel variations in our dataset aided by satellite observations and modelling of atmospheric column CO_2, vegetation growth and soil moisture.

2 | DATA DESCRIPTION AND METHODS

2.1 | Site characteristics

Measurements were carried out on Meteorological Mast 49 at the Mt. Emerald Wind Farm, approx. 50 km SW of Cairns, Queensland, Australia (Figure 1; 17°09′16″ S, 145°21′19″ E, 840 m above sea level). Mt. Emerald is a steep-sided plateau 300 to 400 m above surrounding land. The measurement site has no public access and is approximately 10 km distant from the nearest town or major roads in the predominant upwind direction. The area is at the eastern margin of the Einasleigh Upland Bioregion, immediately west of the Wet Tropics Bioregion and is characterized by open woodland savanna. Rainfall is seasonal with wet season rainfall (November–April) ≈800 mm and dry season rainfall (May–October) ≈50 mm. During the observation period the dominant (83%) wind direction was from the south-eastern quadrant. The 2020–2021 summer (wet season) was characterized by moderate La Niña conditions and rainfall was slightly above the long-term average in NE Queensland (BOM, 2021a).

The northern part of Mt. Emerald is characterized by gently undulating landforms of rhyolite formations, which support poorly developed skeletal soils (RPS Australia East 2011). Rock platforms occasionally break the grass layer. Soils form thin veneers, have low fertility and are mostly poorly drained. Vegetation ground cover is ≈87% (Vegmachine, https://vegmachine.net/) while trees and shrubs (≈20%–30% canopy cover) are dominated by *Eucalyptus spp*. and *Corymbia spp*., typically 2 to 4 m tall with

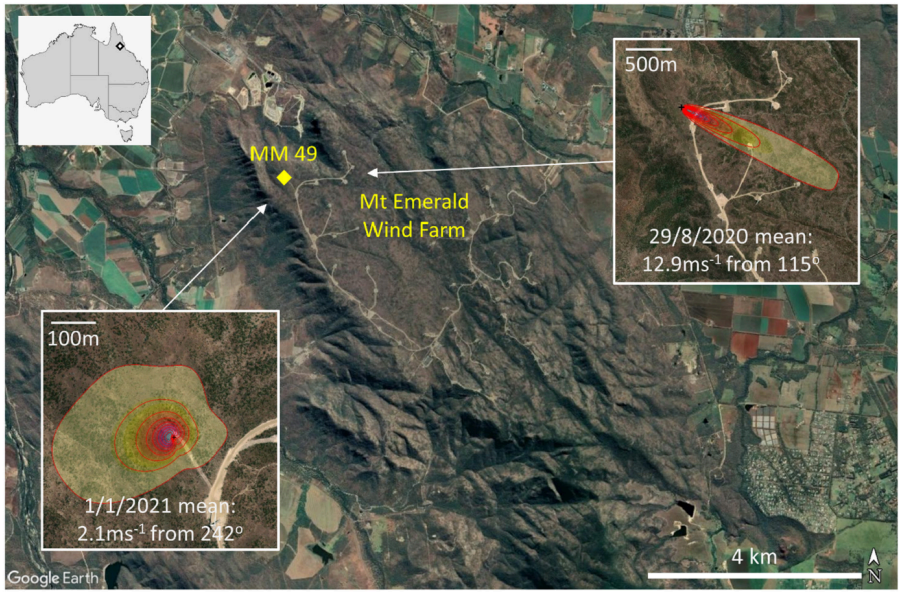

FIGURE 1 Mt. Emerald wind farm and the measurement site at met mast 49 (MM 49). Inserts show mean wind speed and direction and the corresponding land-atmosphere flux footprints for two 24-hr periods calculated according to Kljun et al. (2015, 2021), see text for details. Contour lines show footprint contributions from 10% (inner most) to 90% (outer most) in 10% steps

sparse taller trees to ≈10 m height. Grass trees (*Xanthorrhoea spp.*), typically ≈1 m tall are abundant and Kangaroo grass (*Themeda triandra, Forskk)* is the dominant ground cover across much of the site (RPS Australia East, 2011).

The field campaign was undertaken between 11 June 2020, and 28 May 2021, but was interrupted on 28 September 2020, due to an approaching bush fire, which swept across most of Mt. Emerald. Due to high temperatures during October–November, likely to exceed the instrument operating range, measurements only restarted on 2 December 2020. Additionally, data were lost from 21 February to 5 March 2021, due to equipment failure.

2.2 | Instrumentation

Measurements of CO_2, $\delta^{13}C\text{-}CO_2$, H_2O and CH_4 were carried out using a Picarro G2131i infrared laser spectrometer at 1 Hz (https://www.picarro.com/products). Concentration measurements are reported in parts per million by volume (ppmv) and $\delta^{13}C\text{-}CO_2$ is reported as per mil (‰) deviations from the Vienna Pee Dee Belemnite (VPDB) reference standard scale. Ambient air was pumped at 3 L/min via 3 mm ID FEP tubing from a filtered intake 12 m above ground. A solenoid-operated valve system switched between ambient air and two standard gasses using programmable software. The instrument was housed in a weatherproof, ventilated box and was controlled remotely via a 4G mobile network link.

2.3 | Calibration and data processing

Pressurized cylinders containing dry air with CO_2 concentrations nominally at 384 ± 5 and 483 ± 5 ppmv (BOC Speciality Gasses) were used for CO_2 calibration. The concentrations were determined more accurately by laser spectroscopy (Aerodyne) at the Australian National University's Farquhar Lab at 386.29 ± 0.37 ppmv and 486.36 ± 0.33 ppmv, respectively (mean of 4 determinations before and after the field campaign). The standard gasses were each measured in the field for 30 min. at 30-hr intervals.

The standard gasses were also used to monitor $\delta^{13}C\text{-}CO_2$ drift. The isotope values were determined at ANU to be $\delta^{13}C = -33.42 \pm 0.36$ ‰ and -33.64 ± 0.29 ‰ for the low CO_2 and high CO_2 standards, respectively. In addition to measurement of these standards at 30-hr intervals, calibration of $\delta^{13}C$ values were achieved by measurement of additional standard gasses on-site at 2–4-week intervals. Standard gasses were produced by acidification of four $CaCO_3$ and $NaHCO_3$ powders ($\delta^{13}C$ range − 4.67 to −35.27 ‰) in a custom-built apparatus (Munksgaard et al., 2013) and loaded into a 5-layer Supelco gas bag. The bag was then connected to the analyser and mixed with CO_2 free air to a final concentration in the range 350–450 ppmv for approx. 10–15 min for measurement.

Custom-made software was used to extract data from the instrument log files at 1-min intervals. Calibration equations were generated from all 30-hr standards run within each calendar month. Thirty-minute running averages and daily averages (midnight to midnight) were calculated.

A Licor Li-610 dew-point generator was used to produce H_2O saturated air at 15–24°C to calibrate the Picarro H_2O measurements and verify the dry-air CO_2 concentration calculated by the Picarro instrument. A small additional correction (approximately −0.1 ppmv) was applied to the recorded Picarro dry-air CO_2 data due to a systematic error in the instrument H_2O correction.

Calibration of CH_4 was achieved by measurement of pressurized cylinders containing dry air with 0, 10 and

50 ppmv CH_4 (GasTech Australia) at the start and end of each instrument deployment.

2.4 | Meteorological data

Mt. Emerald Wind Farm operates a comprehensive network of meteorological observations. Wind speed and direction was obtained at 10-min intervals from Met Mast 49 at 32, 61 and 90 m heights above the ground. Air temperature and relative humidity were obtained at 10-min intervals 3 m above the ground. Rainfall data were obtained from Mareeba Airport 10 km NE of Met Mast 49 (BOM, 2021b).

2.5 | OCO-2 CO_2

Regional background CO_2 concentrations from within a 1 x 1 degree box centred on the Mt. Emerald site were obtained from NASA's OCO-2 satellite (Level 2, V9 'lite files', OCO-2 Science Team, 2020) for 17 passes from June 2020 to May 2021. Clouds and/or optically thick aerosols precluded observations during other passes. Data for the layer closest to the ground (≈0–500 m altitude) were used. Individual observations taken at approximately 1–3 s intervals have a footprint ≈1.6 x 2.2 km.

2.6 | Enhanced Vegetation Index (EVI)

Enhanced Vegetation Index (EVI) values were obtained from the Moderate Resolution Imaging Spectroradiometer aboard NASA's Terra and Aqua satellites (product MOD13A1–006, Didan, 2015). Sixteen-day mean values for 500 x 500 m pixels covering the north-western part of Mt. Emerald (Figure 1) were obtained using the Application for Extracting and Exploring Analysis Ready Samples (AρρEEARS) available at https://lpdaacsvc.cr.usgs.gov/appeears/.

2.7 | Soil moisture

Monthly Root Zone Moisture (RZM) levels were obtained from the Australian Water Resources Assessment Landscape model (AWRA-L; BOM, 2021c), which provides the available water as a percentage of the soil water storage capacity in the top 1 m of the soil profile.

2.8 | Data access

The Mt. Emerald spectroscopic and meteorological data are available at.

https://figshare.com/s/9eef6231a818bb27b104
DOI: https://doi.org/10.6084/m9.figshare.17870939.

2.9 | Comments

2.9.1 | Data quality

The precision specification provided by Picarro (https://www.picarro.com/products) for the isotope enabled model G2131i (CO_2 <0.2 ppmv [1σ] 30 s average) is inferior compared to the non-isotopic model G2301 (CO_2 <0.07 ppmv [1σ] 5 s average) commonly used for GHG monitoring in international programs (e.g. ICOS RI, 2020). However, the precision provided by the G2131i was more than adequate to resolve the large diel variations (≈3 to 40 ppmv) in CO_2 concentrations in the present dataset.

Laboratory testing established that the internal precision of the Picarro G2131i used at Mt. Emerald was 0.09 ppmv CO_2 and 0.18 ‰ $\delta^{13}C$ (1σ) for a 1 min running average over a 10-hr period when analysing the high CO_2 standard. During the field campaign the average within-month standard deviation (1σ, $n \approx 25$) of the high (low) CO_2 standard were 0.37 ppmv (0.31 ppmv) CO_2 and 0.30 ‰ (0.29 ‰) $\delta^{13}C$.

The internal precision of the Picarro instrument was 0.008 ppmv CH_4 (1σ) for a 1 min running average over a 6-hr period when analysing the 10 ppmv CH_4 (standard).

2.9.2 | Flux footprint and background air

The Flux Footprint Prediction (FFP) tool of Kljun et al. (2021) was used to calculate the footprint for two 24-hr periods, which represent two extremes of wind speed and direction during the observation period (29/8/2020 during the dry season and 1/1/2021 during the wet season, Figure 1). The estimated footprints are dependent on several input parameters in addition to measurement height (12 m), wind speed and direction (Kljun et al., 2015). Table 1 shows the input parameters used in the calculated examples (values derived from Kljun et al., 2015).

The calculated flux footprints extended a maximum of ≈2 km upwind during the observation period and varied only marginally between convective and stable atmospheric conditions. Given the dominance of SE wind directions at the measurement site (92% during May to September, 74% during December to April) and the homogenous landscape ≈4 km upwind to the southeast, it is unlikely that diel land-atmosphere fluxes beyond Mt. Emerald substantially influenced the measurements at Met Mast 49.

TABLE 1 Input values for flux footprint prediction tool (Kljun et al., 2015, 2021)

Parameter	Value
Displacement height [m] (zm)	1
Obukhov length [m] (L) for convective/stable atm. Conditions	−1000/1000
Standard deviation of lateral velocity fluctuations [ms^{-1}] (σ_v)	1
Friction velocity [ms^{-1}] (u*)	0.5

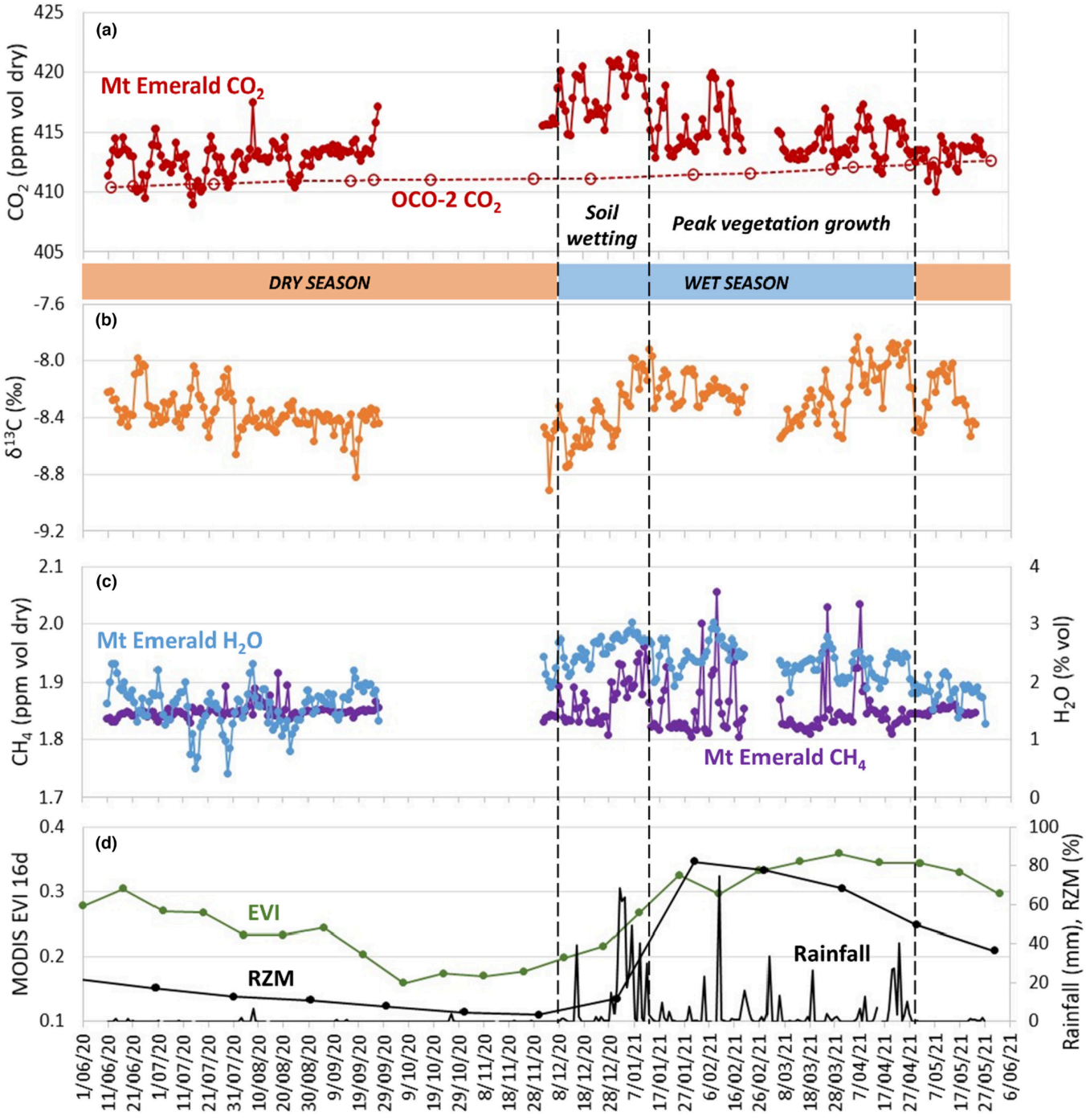

FIGURE 2 Panel (a-c) Daily mean CO_2, CH_4 and H_2O concentrations and $\delta^{13}C$-CO_2 values measured at Mt. Emerald wind farm from June 2020 to May 2021. Panel (a) also shows regional background CO_2 concentrations measured by the OCO-2 satellite (surface layer ≈0–500 m altitude). Panel (d) shows mean 16-day MODIS satellite derived enhanced vegetation index (EVI) values and monthly root zone moisture levels (RZM) derived from the Australian water resources assessment landscape model for Mt. Emerald and daily rainfall observations at Mareeba airport 10 km to the NE of Mt. Emerald (BOM, 2021b)

Estimates of CO_2 concentrations in regional background air at Mt. Emerald, obtained from the OCO-2 satellite data, varied from 410.4 to 412.7 ppmv during June 2020 to May 2021.

2.9.3 | Seasonal variations

Daily average CO_2 concentrations (Figure 2a) ranged from ≈410–415 ppmv during the 2020 dry season from June to September, excluding a few days with concentrations ≈417 ppmv when the site was affected by bushfire smoke. In early-mid December 2020, in response to the first rainfall of the wet season (Figure 2d), daily average CO_2 concentrations rapidly increased to ≈415–422 ppmv, and these values persisted to mid January 2021. Subsequently, daily average CO_2 concentrations were variable, but generally decreased towards the end of the wet season. In May 2021, at the commencement of the dry season, average CO_2 concentrations again ranged from ≈410–415 ppmv. It is notable that the seasonal variations shown in Figure 2a remain nearly unchanged if excluding days with wind directions other than from the SE quadrant (8% from May to September, 26% from December to April). This is a further indication that CO_2 variations were generated locally, and that background CO_2 levels, as recorded by the OCO-2 satellite, were generally well mixed and independent of wind direction.

Average daily $\delta^{13}C$-CO_2 values (Figure 2b) were mostly in the range −8.2 to −8.6 ‰ during the 2020 dry season but generally decreased towards the end of the dry season. After the first seasonal rains in December 2020, $\delta^{13}C$ values increased to ≈−8.0 and then remained in the range −7.9 to −8.5 ‰ for the remainder of the wet season.

Average daily CH_4 concentrations (Figure 2c) varied little during the 2020 dry season (1.84–1.86 ppmv). However, in the 2020–2021 wet season CH_4 concentration increased markedly during and after major rainfall events, peaking at 2.06 ppmv in February 2021, likely due to increasing microbial methanogenesis in the anaerobic zones of waterlogged soils (Le Mer & Roger, 2001).

The Enhanced Vegetation Index (EVI) and Monthly Root Zone Moisture (RZM) values (Figure 2d) increased from mid December 2020 to the end of Jan 2021 in response to wet season rainfall. The increase in CO_2 concentrations within days of the first rainfall of the wet season was likely due to a rapid onset of heterotrophic microbial respiration from the newly wetted topsoils, accumulated plant debris and ash from the late September bush fires. Phenological studies elsewhere have shown that soil respiration generally responds to the initial soil wetting while vegetation greening typically occurs only after several rain events (Moore et al., 2017; Tang et al., 2005; Williams et al., 2009).

As vegetation growth accelerated and photosynthetic activity remained high during the remainder of the wet season to the end of April 2021, plant assimilation of CO_2 resulted in a gradual decline in atmospheric surface concentrations of CO_2 while $\delta^{13}C$ values were elevated because of the preferential plant uptake of $^{12}CO_2$ over $^{13}CO_2$ ('O'Leary, 1988). A gradual decline in CO_2 respired from soil and plant debris following the initial wetting phase may also have contributed to the decrease in atmospheric CO_2 concentration.

2.10 | Diel variations

The dry and wet season diel variations in CO_2 concentration and $\delta^{13}C$-CO_2 values usually followed different general trajectories, although diel patterns during longer relatively dry periods within the wet season resembled those typical of the dry season. Figure 3 shows the 30-min moving averages displayed at 1-min intervals for four representative 5-day periods chosen to show the range and diversity of diel patterns. During the dry season (Figure 3) CO_2 concentrations and $\delta^{13}C$ values varied regularly between night (maximum CO_2, minimum $\delta^{13}C$ values) and day (minimum CO_2, maximum $\delta^{13}C$ values); the $\delta^{13}C$ values increased rapidly mid-morning and decreased rapidly late afternoon. In contrast, in the wet season, diel variations of CO_2 concentrations and $\delta^{13}C$ values (Figure 3), while retaining the same general patterns, were noticeably less regular. It is also apparent that in both dry and wet seasons, CO_2 concentrations and $\delta^{13}C$ values did not always vary in concert.

The contrasting diel patterns of CO_2 concentrations and $\delta^{13}C$-CO_2 values between dry and wet seasons were likely related to seasonal differences in meteorological conditions at Mt. Emerald. During the dry season periods shown in Figure 3, daily average (6–10 m/s) and maximum (10–14 m/s) wind speeds were substantially higher than in the wet season (average 3–6 m/s, maximum 6–10 m/s). The higher wind shear in the dry season can be expected to cause deeper turbulent mixing of the surface atmosphere than in the wet season. In addition, stronger nocturnal radiative cooling in the dry season, when cloud cover is low, may have promoted down-valley cold air drainage (Goulden et al., 2006; Pypker et al., 2007) enhancing vertical air mixing over the plateau as drained air was replaced by air from higher altitude. Consistent with this scenario, typical nocturnal minimum temperatures at Met Mast 49 were lower in the dry season (12–16°C) than the wet season (19–21°C).

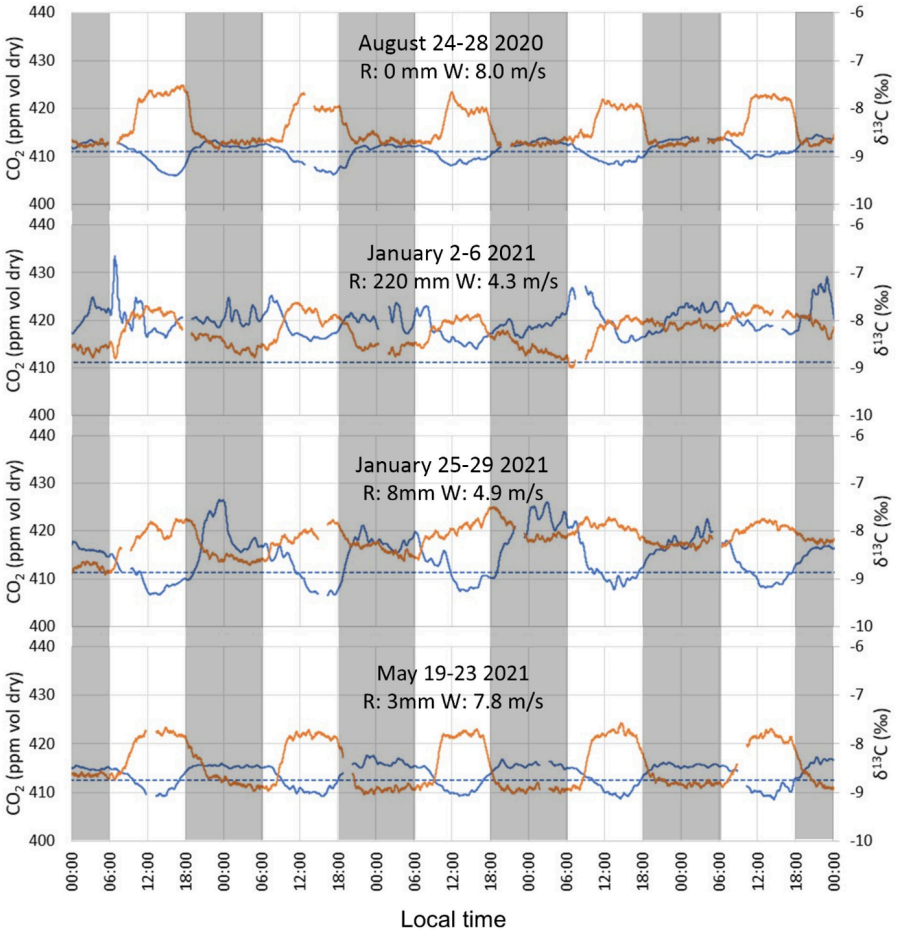

FIGURE 3 Diel variations in CO_2 concentration (blue) and $\delta^{13}C$-CO_2 values (orange) for four 5-day periods (mid dry season 24–28 August 2020; wet season 2–6 January and 25–29 January 2021; early dry season 19–23 May 2021. Data shown are 30 min moving averages displayed at 1 min intervals. Data gaps occur every 30 hr due to measurement of gas standards. The broken blue line represents the regional background CO_2 concentrations obtained by NASA's OCO-2 satellite from approx. 0–500 m altitude within a 1 x 1 degree box centred on Mt. Emerald. Total rainfall (R) and average wind speed (W) are shown for each period

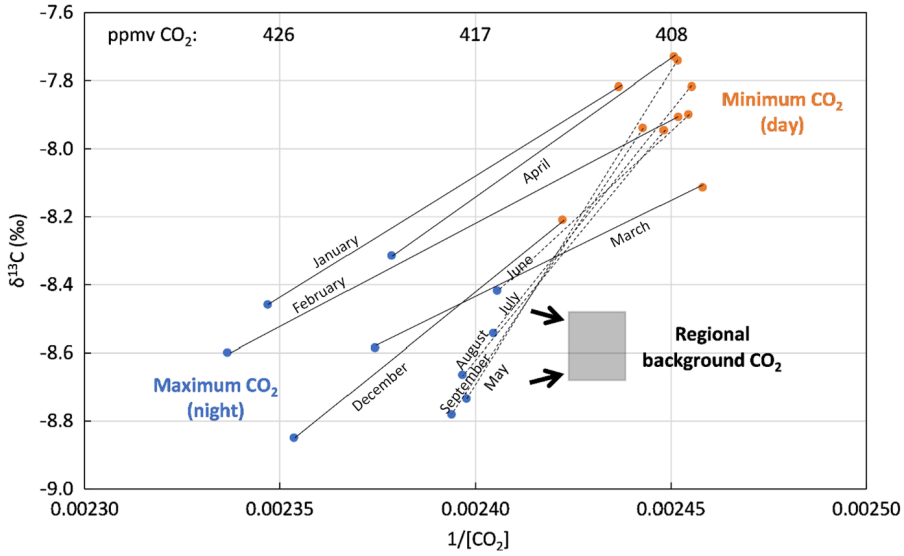

FIGURE 4 Keeling plot showing monthly averages of daily minimum (day) and maximum (night) CO_2 concentrations and corresponding $\delta^{13}C$-CO_2 values. The minimum-maximum ranges (December–April broken lines; May-September full lines) represent the alternating effect of photosynthetic assimilation and respiration of CO_2, which dominates in the wet season (December-April). During the dry season (May–September) additional mixing (arrows) with regional background air from higher altitude (grey box) is driven by stronger wind and nocturnal cold air drainage. The regional background CO_2 box is based on OCO-2 CO_2 concentrations (≈0–500 m altitude) and $\delta^{13}C$-CO_2 values from marine air sampled at Cape Ferguson ≈280 km SE of mt. emerald ($\delta^{13}C = -8.49$ to -8.68, WDCGG, 2021)

A Keeling plot (Pataki et al., 2003) illustrates how mixing between different air parcels with discrete characteristics during the dry and wet seasons may explain the diel CO_2 and $\delta^{13}C$-CO_2 patterns (Figure 4). Monthly averages of daily minimum (day) and maximum (night) CO_2 concentrations and corresponding $\delta^{13}C$-CO_2 values reflect the alternating effect of photosynthetic assimilation and respiration of CO_2, which dominated in the wet season (December–April). The Keeling plot $\delta^{13}C$ intercepts of the wet season monthly linear fits range from −22 to −31 ‰ indicating that the isotopic composition of atmospheric surface CO_2 was moderated by isotopic signals from a mixed C_3-C_4 plant community typical of savanna ecosystems, with C_3 being dominant. Most C_3 plants (savanna trees) have $\delta^{13}C$-CO_2 values in the range from −24 to −31 ‰ while most C_4 plants (savanna grasses) range from −11 to −15 ‰ (O'Leary, 1988).

The CO_2 and $\delta^{13}C$-CO_2 diel variations in the wet season (Figure 4) were thus dominated by two-component mixing of surface air influenced by CO_2 assimilation (day) and respiration (night). The proportional contribution of these sources varied during the diel cycle depending on the relative activity of photosynthetic assimilation – in turn, governed by light, temperature and water availability – and soil/plant respiration. Varying cloud cover and rainfall also influenced the strength of assimilation and respiration and contributed to pattern noise.

In general, wind speeds are higher in the dry (trade wind) season compared to the wet season. This results in a relatively well-mixed lower atmosphere, at day and night on windy days. Additionally, during periods of low cloud coverage, prevalent during the dry season, nocturnal radiative boundary cooling promotes advection of higher altitude air to the measurement site (cold air drainage, see for example Goulden et al., 2006, Pypker et al., 2007). Both these effects are expected to promote stronger mixing of higher altitude air as an additional component to surface air influenced by CO_2 assimilation (day) and respiration (night). This three-component mixing would explain the lower nocturnal CO_2 concentrations, but similar $\delta^{13}C$-CO_2 values, in the dry season compared to the wet season (Figure 4). The general absence of clouds and rainfall in the dry season resulted in more regular diel patterns compared to the wet season.

3 | CONCLUSIONS

The Mt. Emerald spectroscopic data provide a detailed characterization of atmospheric surface concentrations of CO_2 and CH_4 at a tropical savanna site over 1 year. CO_2 isotope data and meteorological observations further strengthens the utility of the data for future modelling studies. Seasonal and diel variations in CO_2 concentrations and $\delta^{13}C$-CO_2 values were primarily controlled by local microbial soil respiration and plant photosynthetic assimilation while mixing with higher altitude regional background air played a secondary role in the dry season. Concentrations of CH_4 increased markedly during and after major rainfall events when the ground became waterlogged.

AUTHOR CONTRIBUTIONS

Niels Crosley Munksgaard: Conceptualization (equal); data curation (lead); formal analysis (lead); investigation (lead); methodology (lead); software (equal); writing – original draft (lead); writing – review and editing (equal). **Ickjai Lee:** Investigation (supporting); methodology (supporting); software (equal); writing – review and editing (equal). **Thomas Napier:** Investigation (supporting); methodology (supporting); software (equal); writing – review and editing (equal). **Costijn Zwart:** Formal analysis (supporting); investigation (supporting); methodology (supporting); software (equal); writing – review and editing (equal). **Lucas A. Cernusak:** Conceptualization (supporting); formal analysis (supporting); funding acquisition (equal); investigation (supporting); methodology (supporting); writing – original draft (supporting); writing – review and editing (equal). **Michael Bird:** Conceptualization (equal); formal analysis (supporting); funding acquisition (equal); investigation (supporting); methodology (supporting); writing – original draft (supporting); writing – review and editing (equal).

ACKNOWLEDGEMENTS

We thank Paul McDonald (RATCH-Australia Corporation Pty Ltd) for access to Mt. Emerald Wind Farm and providing meteorological data, Dr. Hilary Stuart-Williams (Australian National University) for analysis of standard gasses, Dr. Paul Krummel (CSIRO) for providing GHG data from Cape Ferguson, Esq. Douglas Alexander (Sandy) Southwood and Dr. Han She Lim for field assistance.

FUNDING INFORMATION

Australian Research Council Grant LE110100144.

OPEN RESEARCH STATEMENT

This article has earned an Open Data badge for making publicly available the digitally-shareable data necessary to reproduce the reported results. The data is available at https://doi.org/10.6084/m9.figshare.17870939. Learn more about the Open Practices badges from the Center for Open Science: https://osf.io/tvyxz/wiki.

DISCLOSURE

The authors declare no conflict of interest.

ETHICS APPROVAL

Ethics approval was not required for this project.

ORCID

Niels C. Munksgaard https://orcid.org/0000-0003-4906-1544
Ickjai Lee https://orcid.org/0000-0002-6886-6201
Thomas Napier https://orcid.org/0000-0003-4218-6731
Costijn Zwart https://orcid.org/0000-0002-2450-0531
Lucas A. Cernusak https://orcid.org/0000-0002-7575-5526
Michael I. Bird https://orcid.org/0000-0003-1801-8703

REFERENCES

Agustí-Panareda, A., Diamantakis, M., Massart, S., Chevallier, F., Muñoz-Sabater, J., Barré, J. et al. (2019) Modelling CO_2 weather – why horizontal resolution matters. *Atmospheric Chemistry and Physics*, 19, 7347–7376. Available from: https://doi.org/10.5194/acp-19-7347-2019

Bureau of Meteorology (2021a) Australia in summer 2020–21. Available from: http://www.bom.gov.au/climate/current/season/aus/archive/202102.summary.shtml [Accessed 20th December 2021].

Bureau of Meteorology (2021b) Mareeba, Queensland Daily Weather Observations. Available from: http://www.bom.gov.au/climate/dwo/IDCJDW4080.latest.shtml [Accessed 20th December 2021].

Bureau of Meteorology (2021c) Australian Landscape Water Balance. Available from: http://www.bom.gov.au/water/landscape/#/sm/Actual/day/-28.4/130.4/3/Point/2021/12/19/ [Accessed 20th December 2021].

Didan, K. (2015) MOD13A1 MODIS/Terra vegetation indices 16-day L3 global 500m SIN grid V006 [data set]. NASA EOSDIS Land Processes DAAC. https://doi.org/10.5067/MODIS/MOD13A1.006. [Accessed 20th December 2021].

Goulden, M.L., Miller, S.D. & da Rocha, H.R. (2006) Nocturnal cold air drainage and pooling in a tropical forest. *Journal of Geophysical Research*, 111, D08S04. Available from: https://doi.org/10.1029/2005JD006037

Graven, H., Allison, C.E., Etheridge, D.M., Hammer, S., Keeling, R.F., Levin, I. et al. (2017) Compiled records of carbon isotopes in atmospheric CO2 for historical simulations in CMIP6. *Geoscientific Model Development*, 10, 4405–4417. Available from: https://doi.org/10.5194/gmd-10-4405-2017

Haverd, V., Raupach, M.R., Briggs, P.R., Canadell, J.G., Davis, S.J., Law, R.M. et al. (2013) The Australian terrestrial carbon budget. *Biogeosciences*, 10, 851–869. Available from: www.biogeosciences.net/10/851/2013/

Haverd, V., Raupach, M.R., Briggs, P.R., Canadell, J.G., Davis, S.J., Law, R.M. et al. (2015) Corrigendum to "the Australian terrestrial carbon budget" published in biogeosciences, 10, 851–869, 2013. *Biogeosciences*, 12, 3603–3605. Available from: www.biogeosciences.net/12/3603/2015/

ICOS RI (2020) ICOS Atmosphere Station Specifications V2.0 (editor: O. Laurent). ICOS ERIC. Available from: https://doi.org/10.18160/GK28-2188.

Kljun, N., Calanca, P., Rotach, M.W. & Schmid, H.P. (2015) A simple two-dimensional parameterisation for flux footprint prediction (FFP). *Geoscience Model Development*, 8, 3695–3713, Available from: www.geosci-model-dev.net/8/3695/2015/

Kljun, N., Calanca P., Rotach, M.W., & Schmid H.P. (2021) A simple two-dimensional parameterisation for Flux Footprint Prediction (FFP). Available from: https://footprint.kljun.net/ [Accessed 20th December 2021].

Le Mer, J. & Roger, P. (2001) Production, oxidation, emission and consumption of methane in soils: a review. *European Journal of Soil Biology*, 37, 25–50. Available from: https://doi.org/10.1016/S1164-5563(01)01067-6

Moore, C.E., Beringer, J., Evans, B., Hutley, L.B. & Tapper, N.J. (2017) Tree-grass phenology information improves light use efficiency modelling of gross primary productivity for an Australian tropical savanna. *Biogeosciences*, 14, 111–129. Available from: https://doi.org/10.5194/bg-14-111-2017

Munksgaard, N.C., Davies, K., Wurster, C.M., Bass, A.M. & Bird, M.I. (2013) Field-based cavity ring-down spectrometry of $\delta^{13}C$ in soil-respired CO_2. *Isotopes in Environmental and Health Studies*, 49, 232–242. Available from: https://doi.org/10.1080/10256016.2013.750606

O'Leary, M.H. (1988) Carbon isotopes in photosynthesis. *Bioscience*, 38, 328–336.

OCO-2 Science Team (2020) OCO-2 level 2 bias-corrected XCO2 and other select fields from the full-physics retrieval aggregated as daily files, retrospective processing V10r. Greenbelt, MD, USA, Goddard, Earth Sciences Data and Information Services Center (GES DISC). Available from: https://doi.org/10.5067/E4E140XDMPO2 [Accessed 20th December 2021].

Pataki, D.E., Ehleringer, J.R., Flanagan, L.B., Yakir, D., Bowling, D.R., Still, C.J. et al. (2003) The application and interpretation of Keeling plots in terrestrial carbon cycle research. *Global Biogeochemical Cycles*, 17, 1022. Available from: https://doi.org/10.1029/2001GB001850

Poulter, B., Frank, D., Ciais, P., Myneni, R.B., Andela, N., Bi, J. et al. (2014) Contribution of semi-arid ecosystems to interannual variability of the global carbon cycle. *Nature*, 509, 600–603. Available from: https://doi.org/10.1038/nature13376

Pypker, T.G., Unsworth, M.H., Mix, A.C., Rugh, W., Ocheltree, T., Alstad, K. et al. (2007) Using nocturnal cold air drainage flow to monitor ecosystem processes in complex terrain. *Ecological Applications*, 17, 702–714.

RPS AUSTRALIA EAST (2011) Mount emerald wind farm, Herberton Range North Queensland. Environmental Impact Statement. Report to Ratch Australia Corporation LTD.

Tang, J., Baldocchi, D.D. & Xu, L. (2005) Tree photosynthesis modulates soil respiration on a diurnal time scale. *Global Change Biology*, 11, 1298–1304. Available from: https://doi.org/10.1111/j.1365-2486.2005.00978.x

Villalobos, Y., Rayner, P., Thomas, S. & Silver, J. (2020) The potential of orbiting carbon Observatory-2 data to reduce the uncertainties in CO2 surface fluxes over Australia using a variational assimilation scheme. *Atmospheric Chemistry and Physics*,

20, 8473–8500. Available from: https://doi.org/10.5194/acp-20-8473-2020

Villalobos, Y., Rayner, P.J., Silver, J.D., Thomas, S., Haverd, V., Knauer, J. et al. (2021) Was Australia a sink or source of CO_2 in 2015? Data assimilation using OCO-2 satellite measurements. *Atmospheric Chemistry and Physics*, 21(23), 17453–17494. Available from: https://doi.org/10.5194/acp-21-17453-2021

WDCGG (2021) World data Centre for Greenhouse Gasses. Available from: https://gaw.kishou.go.jp/ [Accessed 20th December 2021].

Williams, C.A., Hanan, N., Scholes, R.J. & Kutsch, W. (2009) Complexity in water and carbon dioxide fluxes following rain pulses in an African savanna. *Oecologia*, 161, 469–480. Available from: https://doi.org/10.1007/s00442-009-1405-y

How to cite this article: Munksgaard, N.C., Lee, I., Napier, T., Zwart, C., Cernusak, L.A. & Bird, M.I. (2023) One year of spectroscopic high-frequency measurements of atmospheric CO_2, CH_4, H_2O and $\delta^{13}C$-CO_2 at an Australian Savanna site. *Geoscience Data Journal*, 10, 461–470. Available from: https://doi.org/10.1002/gdj3.180